Electron paramagnetic resonance approaches to biologically relevant reactions: examples from a aggregation to enzymes

Passerini, L.

Chapter 3.

Investigating α-Synuclein Aggregation In Situ Using Site-Directed Spin Labeling and EPR

3.1 Introduction

α-Synuclein (αS) is an intrinsically disordered protein with 140 aminoacid residues, which is of major interest due to its involvement in neurodegeneration, particularly in Parkinson's disease (PD) [1-4]. Under pathological conditions, αS aggregates into β-sheet rich structures, called fibrils, whose presence is the histological hallmark in the brain of PD patients.

The aggregation of αS is a complex process that involves the formation multiple intermediates, including oligomers, identified as the toxic species taking part in the neurodegeneration, before the mature fibrils are formed [3, 5, 6].

While fibrils are particularly stable structures, and have been extensively characterized by CryoEM and ssNMR [7-13], characterization of oligomers is challenging due to their transient nature and structural heterogeneity [14, 15]. Methods for oligomer characterization often involve chemical modification or dilution for single-molecule experiments [14, 16-21], which can stabilize only specific structures, and potentially distort the natural equilibrium of the aggregation process.

A widely used method to monitor αS aggregation is the Thioflavin T (ThT) fluorescence assay, which allows to specifically detect β-sheet-rich fibrillary aggregates, but does not provide direct information on monomers or early stage intermediates like oligomers [5, 22-24]. A typical ThT fluorescence curve follows a sigmoidal trend: It begins with a lag phase, during which no fluorescence is detected and oligomers and intermediates are forming. The lag phase is followed by an exponential increase as the β-sheet fibrils start to assemble, and ending in a plateau where the system reaches equilibrium [5, 22]. However, since ThT fluorescence only tracks fibrils, it lacks the ability to resolve non-fibrillar species, making it unsuitable to monitor early aggregation events.

Recently, Zurlo et al. [25], developed an approach to investigate αS aggregation in situ using site-directed-spin-labeling (SDSL) and continuous wave electron paramagnetic resonance (CW-EPR) (figure 1)[25]. The key advantage of this method is that it directly measures the mobility of the protein in solution, with different species giving distinct EPR spectral shapes. By measuring the aggregating solution directly, the EPR spectra contain information on all species present, from monomers to oligomers and fibrils. By simulating the EPR spectra with three components, each with a different rotational correlation time (τ_r), the contributions of the different species were disentangled and quantified, giving quantitative information on the amount of monomers, oligomers and fibrils in solution. The study identified an early oligomeric population in equilibrium with monomers, leading to a kinetic model in which oligomers could either serve as precursors to fibrils or dissociate back into monomers [25]. The oligomers identified had a relatively fast dissociation rate, making them impossible to detect with techniques that require separation of species or dilution, making in situ EPR a powerful method for the identification of such metastable, short lived species.

To ensure comparability between different aggregation assays, ThT fluorescence assays must be run in parallel with EPR measurements, allowing direct correlation between fibril formation and EPR spectral changes. Another challenge in applying this method is that the EPR spectral components from different species overlap, making it difficult to unambiguously distinguish the spectral contribution of oligomers from that of fibrils [26]. Also, a three-component simulation may be overfitting the data that suffer from low resolution, especially when the intensities of the long-τ_r components are low, such as at the beginning of the aggregation. In this study, we simplify the analysis by employing a two-component model, where the τ_r of monomers is obtained from monomeric αS and the τ_r of aggregates is determined from fibril-enriched samples. This approach reduces potential fitting bias and improves reproducibility while still allowing the detection of early aggregates. Additionally, we introduce confidence intervals in quantifying component contributions, providing a more robust assessment of the species present in solution.

Another challenge in in situ EPR analysis is label dissociation, which can complicate spectral interpretation [25, 26]. The most commonly used nitroxide spin label, MTSL, forms a disulfide bond with cysteine residues (figure 2) that is susceptible to reduction over time, resulting in a considerable amount of free label contributing to the spectral shape. To address this, we compare multiple spin labels with different chemical linkages, assessing their stability during aggregation (figure 2).

To probe structural features of aggregates, we introduce spin labels at different positions in the αS sequence. By monitoring the time evolution of EPR spectral components for spin labels at position 9, 27 and 56, we show that in situ EPR can reveal how specific regions of αS integrate into aggregates, providing valuable insights into early-stage oligomerization.

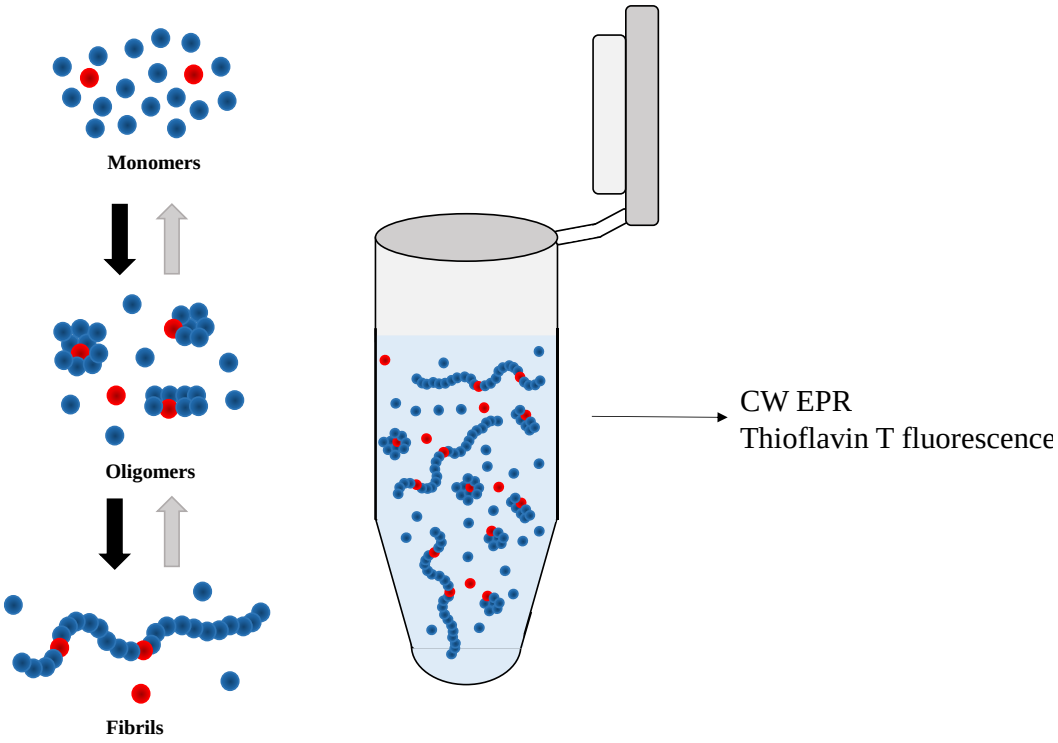

Figure 1. Overall aggregation pathway and depiction of in situ EPR method. Spin labelled αS (red dots) is diamagnetically diluted with wt αS (blue dots). The aggregating sample, containing monomers, oligomers and fibrils is measured directly with CW EPR and ThT fluorescence.

3.2 Materials and Methods

Protein Labeling, Preparation, Aggregation Conditions

Protein expression and purification were as described in Zurlo et al [25]. The spin labels were all purchased by Toronto Research Chemicals. The spin labels used were: MTSL (*S*-(1-oxyl-2,2,5,5-tetramethyl-2,5-dihydro-1H-pyrrol-3-yl)methyl methanesulfonothioate), IAP (3-(2-Iodoacetamido)-2,2,5,5- tetramethyl-1-pyrrolidinyloxy) and MAP (3-Maleimido,2,2,5,5-tetramethyl-1-pyrrolidinyloxy). The labeling was performed as described in Zurlo et al. [25], with variation on the incubation conditions with the label: the incubation with the labels was performed overnight at 4 °C with gentle shaking. Although the protein stocks were purified and monomeric, this was not tested immediately before starting the aggregation experiment, and therefore a small population of multimeric species cannot be excluded. Description of experiment: a stock solution of spin-labeled α-synuclein was diluted into 1 mL

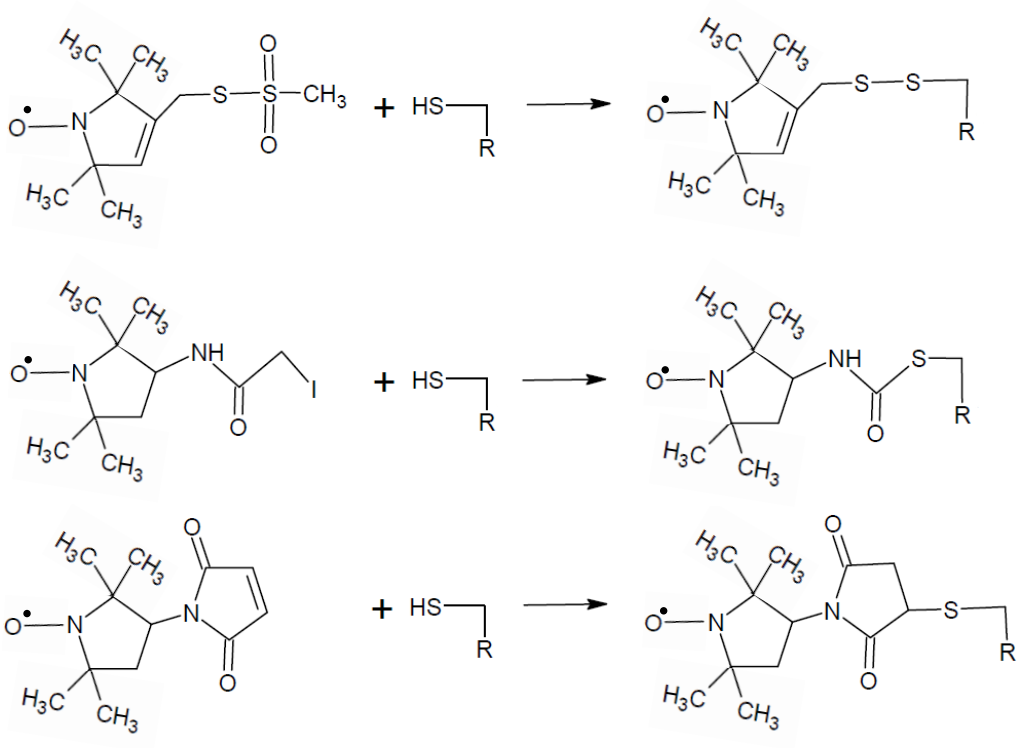

Figure 2. Structures and labeling reactions of the spin labels used in this work. A) MTSL (R1) B) MAP (R2) C) IAP (R3).

of assay buffer (10 mM Tris–HCl, pH 7.4, 0.01% NaN_3), to a final spin concentration of 10 µM. The solution also contained wild-type α-synuclein (wt-αS) for a total α-synuclein concentration of 100 µM. The solutions were prepared in 1.5 mL low bind Eppendorf tubes. After an initial EPR and fluorescence measurement was taken at the time the spin labeled protein was diluted, the samples were allowed to aggregate on a thermomixer (Eppendorf, Thermomixer comfort) with a speed of 1000 rpm at 37 °C. At each time point, 30 µL samples were drawn from the aggregation solution and used for EPR and Thioflavin T (ThT) fluorescence assay. Samples needed to be measured once extracted, as storage at room temperature might allow aggregation to proceed, and fibril denaturation has been proved at low temperatures [27]. This ultimately limits to one, maximum two, aggregating samples that can be run simultaneously.

Diamagnetic Dilution

To suppress changes in the EPR lineshape by spin–spin interactions, all samples were made with a mixture of 9:1 wild type αS: spin-labelled αS, as described in [25].

Thioflavin T fluorescence assay

Thiofavin T (ThT) fuorescence measurements were made by diluting 10 µL of the aggregating solution in 1 mL assay buffer with 5 µM ThT. Measurement were carried out on a Varian Cary Eclipse Fluorescence Spectrophotometer (Varian, Palo Alto, US). Excitation wavelength was set to 440 nm and emission spectra were recorded between 460 and 600 nm. The fluorescence intensity at the 485 nm maximum was recorded. ThioT fluorescence measurement can be subject to fluctuations once the plateau phase is reached. To improve readability of the time traces shown in main text, some of the ThioT fluorescence time points were removed from the plots. This was only done once the curve reached the plateau phase, so the time points in the lag phase and exponential growth phase are not affected.

EPR Measurement Conditions

For the EPR measurements, glass micropipettes of a volume of 50 µL (Blaubrand Intramark, Wertheim, Germany) were filled with 20 µL of the sample for each measurement. The 9 GHz, continuous-wave EPR spectra were recorded using an EMX Plus spectrometer (Bruker, Rheinstetten, Germany). The measurements conditions were: room temperature, microwave power 2.0 mW, modulation amplitude 0.25 mT or 0.5 mT, modulation frequency 100 kHz, time constant 20.48 ms. The high modulation amplitude (0.5 mT) was in some cases used to enhance broad, low intensity components. The time spent on each measurement was adapted according to the spectral lineshape, i.e., the aggregation time, and they could last from 20 minutes to 1 hour. The spin concentration was determined by comparing the double integral of the EPR spectra with the double integral of a reference sample in buffer (label concentration 100 µM). The spin concentrations were ≈ 10 µM for a total protein concentration of 100 µM.

Preparation of fibril enriched sample

To prepare a fibril enriched sample, 300 µL of the aggregating solution were centrifuged with an airfuge (Beckman Coultier, Brea, USA) at 65000 rpm for ten minutes. The surnatant was removed, and the pellet re-suspended in assay buffer. The procedure was repeated three times, after which most of the monomers and free label were removed from the solution. Finally, 20 µL of the re-suspended pellet were used for EPR measurement as described in “EPR measurement conditions”.

Simulations of EPR Spectra

EPR spectra were baseline corrected using WinEPR software (Bruker, Reinstetten, Germany). MATLAB (version 9.4.0.813654, R2019a, The MathWorks, Inc., Natick, MA, USA) and the EasySpin package (5.3.5) were used for simulations of the EPR spectra [28]. The simulations were performed as described by Zurlo et al. [25]: the parameters of the simulation were manually adjusted to agree best with the experimental spectra. For all simulations, an isotropic rotation of the nitroxide (S=1/2) and a common set of g- and A-tensor principal values were used: g = [2.0090 2.0068 2.0030], A = [13 13 109] MHz. A superposition of three components was used, simulated with the "chili" function and differing based on rotational correlation time. The τ_r obtained at t=0 was kept constant for all other simulations as the correlation time for the fast (monomer) fractions. The τ_r for aggregates was derived from spectra acquired from fibril enriched samples. The error margins on the correlation time used for simulation of the slow component are determined by manually adjusting the τ_r, until the simulation was not a good fit for the experimental spectrum anymore. A very fast component was assigned to free label. The τ_r values of each of the fractions were kept constant for the entire series. For each time point, the relative contribution of the components was optimized. In [25], a component was used to define medium sized aggregates. In this work, the approach presented in Zurlo [25] is simplified to include two components, eliminating the component with intermediate τ_r. In the early stages of the aggregation, the signal-to-noise ratio of the broad component is low, and a wide range of τ_r can be used to simulate the spectrum, including the τ_r used for simulation of fibril enriched spectra. Error margins on τ_r and on the contribution of the EPR component to the spectrum were derived by manually adjusting the simulation parameters, until they would not reproduce the experimental spectrum anymore. The data presented in this work for aS56R1 were collected in our laboratory and previously published in [25], and were reanalyzed in the present study with the updated analysis method.

3.3 Results

The aggregation of α-Synuclein (αS) is probed by site-directed-spin-labeling (SDSL)-EPR and Thioflavin T (ThT) fluorescence, as described in Materials and methods. The protein was labelled with MTSL (*S*-(1-oxyl-2,2,5,5-tetramethyl-2,5-dihydro-1H-pyrrol-3-yl)methyl methanesulfonothioate) in position S9 (αS9R1), A27 (αS27R1) and A56 (αS56R1). Also two other labels, MAP (3-Maleimido,2,2,5,5-tetramethyl-1-pyrrolidinyloxy) and IAP (3-(2-Iodoacetamido)-2,2,5,5- tetramethyl-1-pyrrolidinyloxy), were probed, in position 56. The two spin-label variants are referred to αS56R2 (IAP) and αS56R3 (MAP). All experiments are performed with a 9:1 mixture of αS wt and the spin labelled αS variant, respectively. To

illustrate the overall behavior of the spectra and the analysis, we first describe the results for αS56R1, next, the results of the different label positions and the different labels are described.

Figure 3 shows the spectra acquired at different time points of the aggregation of αS56R1. The spectra are dominated by the classical three-line component observed for nitroxides in fast motion, where the three lines arise from the interaction of the unpaired electron spin with the nearby ^{14}N nucleus. Over time, a spectral component with a broader linewidth appears, coming from species with larger rotational correlation times (τ_r), and the intensity of broad component relative to the narrow line component increases during the incubation. Spectral simulation was performed to determine the correlation time and the relative contribution of such components to the EPR lineshape. The spectra were simulated using two components, designated as “fast” and “slow”, which are shown in figure 4A. The fast component is attributed to monomeric αS, and its τ_r was obtained from the EPR spectrum acquired before the start of the aggregation. The slow component is assigned to aggregates, and its τ_r was determined from a fibril- enriched sample, prepared as described in Materials and methods (see SI for fibril spectra). All the spectra acquired for different mutants and labels were simulated with this two-component model. The rotational correlation times for the different spectral components in all samples are given in table 1, and the remaining parameters in Materials and methods. All experimental spectra and simulations are shown in the SI.

By simulating the spectra acquired over the time of the incubation, the time developments of the contribution for the fast and slow components were extracted. Figure 4B shows the time development of the EPR components for αS56R1, alongside the ThT fluorescence intensity. In figure 4B, the contribution of the fast component decreases over time, while the slow component increases, reaching a plateau at later stages of aggregation. It can be noticed that the slow component is already present at early times of the incubation, in the first 15 hours, when the ThT assay is not detecting any fibrillary aggregates yet. A similar time evolution was observed for αS9R1 and αS27R1 as shown in figure 5.

A direct comparison of the development of the slow component over time of αS56R1, αS9R1 and αS27R1 is given in figure 6A. During the early stages of aggregation (first ten hours), the

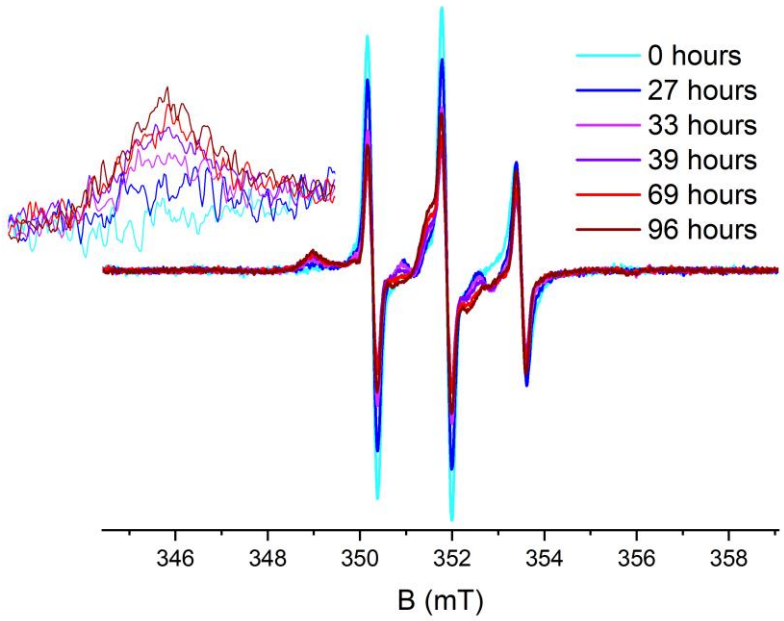

Figure 3. EPR spectra obtained at different time points during the aggregation of aS56R1. In the inset, a zoom-in of the broad spectral component arising from aggregates. Spectra are normalized to double

slow- component contribution is higher for αS27R1, compared to αS56R1 and αS9R1. However, at later stages of aggregation, αS9R1 reaches a plateau after 75 hours, later than αS27R1 and αS56R1, for which the plateau is developed after 50 hours of incubation. The ThT fluorescence curves for all mutants (figure 6C), show no significant differences.

Figure 6B and D show the comparison of the development of slow components and ThT curves for different labels (MTSL-R1, MAP-R2 and IAP-R3) for the A56C mutant. No significant differences are observed between αS56R1 and αS56R2. In contrast, deviations occur in the case of αS56R3, where the exponential growth phase stops after 20 hours of incubation, to resume and reach a plateau after 75 hours of incubation. For αS56R3, ThT shows that the aggregation itself is delayed relative to R1 and R2. As all samples contain only 10% of the labelled protein, the delay for R3 is unlikely related to the spin-label structure and we attribute it to a random change in aggregation.

In all samples, an additional very fast (very short τ_r) component is present in the EPR spectrum. The τ_r is such that it can only be due to free label. In figure 7, the time development of the free-label component is given for the different labels used, and in the SI it is given also for αS9R1 and αS27R1. For αS56R1, the free-label component increases over time, suggesting detachment of the label from the protein. This effect is even more pronounced for αS56R3, where the free label component accounts for almost 60% of the spectral lineshape after 200 hours of aggregation. In contrast, for αS56R2, the free label component remains constant during the incubation, suggesting that free spin label was already present at the start of the incubation, rather than detaching over time.

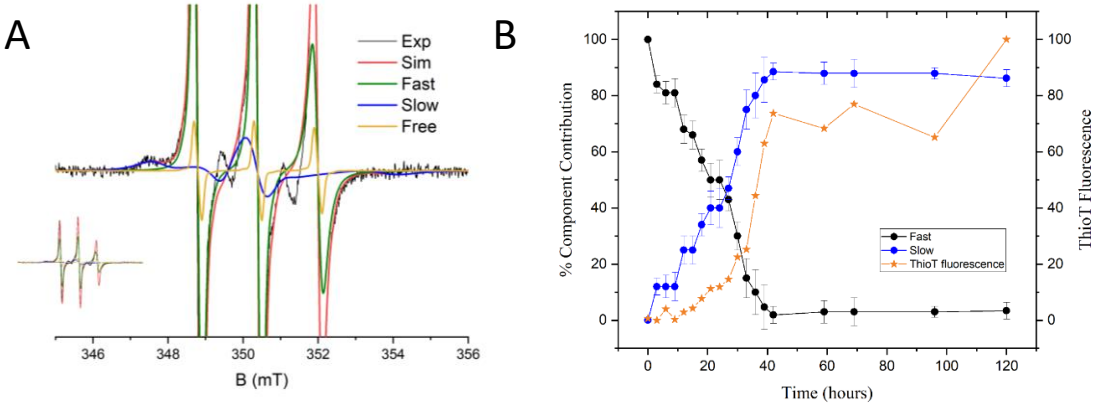

Figure 4. Overview of the aggregation process. EPR spectra, simulation components and time development of simulation components for αS56R1. The experimental spectrum simulated here is obtained after 18 hours of incubation. A) Simulation performed with fast and slow components. Inset: full spectrum. B) Time development of the fast and slow components shown in A). An additional component with the correlation time of free label in solution appears over time, and is added to the simulation. A): black: experimental spectrum. Red: total simulation. Green: fast (monomer) component. Blue: slow (aggregates) component. Yellow: free label component. The data presented in this figure were collected in our laboratory and previously published in [25].

Table 1. Rotational correlation times used for simulation of fast, medium and slow components. The monomer correlation times are obtained from monomer spectra. The correlation times of fibrils are obtained from a fibril enriched sample. For details, see main text

	Monomer τ_r (ns)	**Fibril τ_r (ns)**
αS56R1	0.41	7.28 ± 1.34*
αS56R3	0.31	7.04 ± 1.45
αS56R2	0.38	6.6 ± 1.86
αS27R1	0.40	6.35 ± 1.46
αS9R1	0.37	7.94 ± 0.7

*The rotational correlation time used in [25] for the slow fraction is 10 ns.

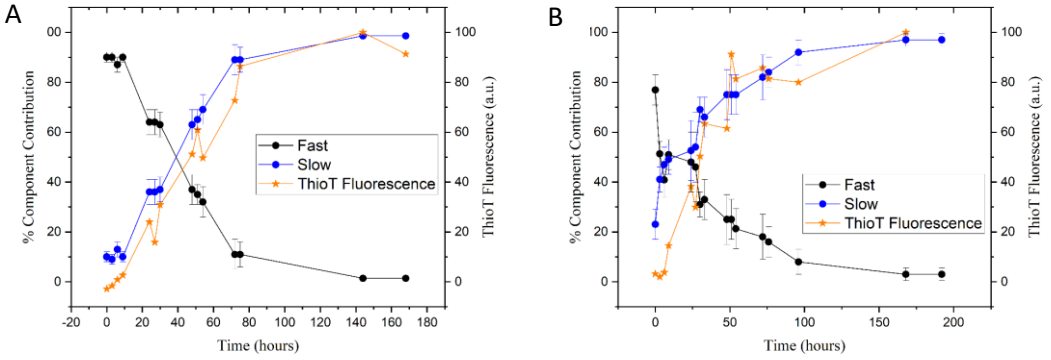

Figure 5. Development of ThioT fluorescence and EPR simulation components over time, for αS9R1 mutant (A) and αS27R1 mutant (B). The solid lines are a guide to the eye.

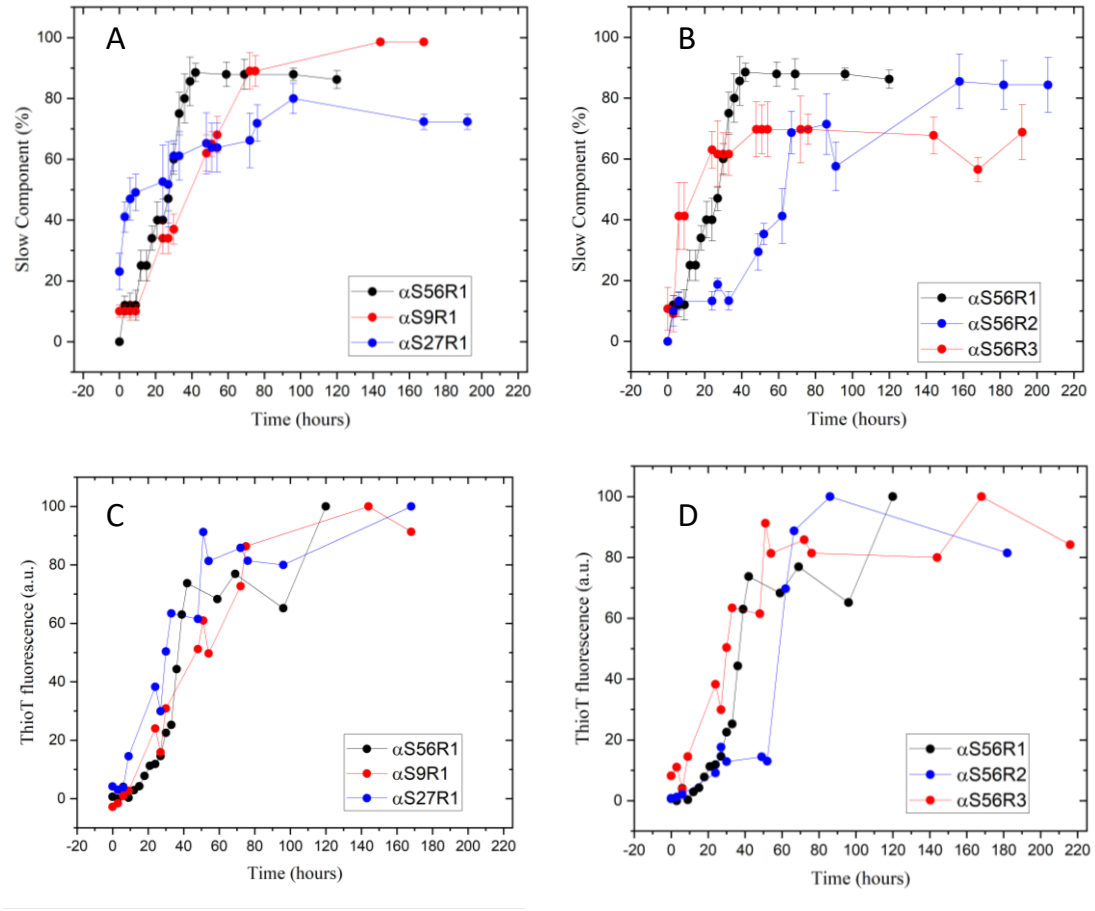

Figure 6. Comparison of the time development of slow component for different mutants (A) and labels (B). Comparison of ThioT fluorescence curves for different mutants (C) and different labels (D).

3.4 Discussion

The method of monitoring αS aggregation in situ with EPR was first reported by Zurlo et al, with αS labelled in position 56 [25]. Here, we extended the investigation to probe the positions 9 and 27, and two additional types of spin labels. In addition, the data were analyzed with improved simulations, providing a more systematic investigation of the in situ αS aggregation by SDSL EPR.

The aggregation is monitored by the CW EPR spectrum, which is sensitive to the τ_r of the nitroxide moiety. The local mobility of the bonds linking the nitroxide to the protein backbone, see figure 2, together with the flexibility of αS, are dominating the spectral line shape. In its monomeric form, αS has a spectrum characteristic of a relatively fast rotating nitroxide (see figure 3). If αS aggregates, the nitroxide rotation becomes hindered by the interaction of the label with other monomers, leading to a longer τ_r and spectral broadening. During aggregation, spin labels may come in close proximity within the aggregates, leading to spectral broadening due to spin-spin interactions, such as exchange coupling. To prevent this effect and ensure that spectral changes reflect differences in mobility rather than label-label interactions, the labeled protein is diluted with wild-type αS (diamagnetic dilution), increasing the average nitroxide-nitroxide distance within the aggregates.

Figure 1 shows that amyloid aggregation involves the formation of multiple aggregate species that differ in structure and size. In the course of incubation, aggregates form and the spectra will be a superposition of the spectra of all these different aggregates present in solution. As the spectra of these aggregates are expected to differ, at least three different mobility components (figure 1), with distinct τ_r, corresponding to monomers, intermediates and fibrils are expected. For two of these components, τ_r values can be determined experimentally (monomers and fibrils, see results). In Zurlo et al. [25] three components were used, one for monomers, one for intermediates and one for fibrils. However, the τ_r for intermediate species cannot be directly extracted from experimental data, and, as shown in [26], the τ_r values of intermediates and fibrils overlap within uncertainty margins, making their spectral contributions interchangeable.

Extensive analysis of the data and testing different simulation parameters revealed that the τ_r experimentally determined from fibrils can be used to simulate the spectral component observed at early time points, where its contribution is weak relative to the overall spectrum. Given the larger dataset obtained in the present study and the need to streamline the analysis while avoiding bias, we opted for this more robust model. By using the τ_r obtained from fibrils to represent all aggregated species, both intermediates and fibrillary aggregates contribute to the same EPR spectral component. However, only fibrils show ThT

fluorescence, so by monitoring the aggregation with ThT in parallel to the EPR experiments, the non-ThT active contribution of the oligomers is identified.

Structural information from in situ EPR

In principle, EPR can provide local structural information by revealing how specific regions of a protein are incorporated into an aggregate. Therefore, by labeling different positions (9, 27 and 56) in the present study, variations in immobilization within the aggregates can be observed and offer insights into structural features of the aggregates.

As for fibrils there is independent information on structure [7-13], we test the ability of the EPR approach to obtain such structural information. It is known [7-13], that in the fibril state position 56 is situated in the fibril core, while 9 and 27 are positioned on the outside of the fibrils, suggesting that the αS positions studied in the present work reflect these differences. For this reason, position 9 and 27 were expected to have a higher mobility in EPR, i.e. shorter τ_r, than position 56. However, the τ_r of the slow (fibril) component is, within error margins, the same for the different mutants analyzed (see table 1 for correlation times, and SI for spectra). This suggests that EPR at 9 GHz does not have sufficient resolution to differentiate between the αS positions investigated here.

What we observed, however, is that the time development of the slow component is different in the different mutants, suggesting that the time course of the development of the

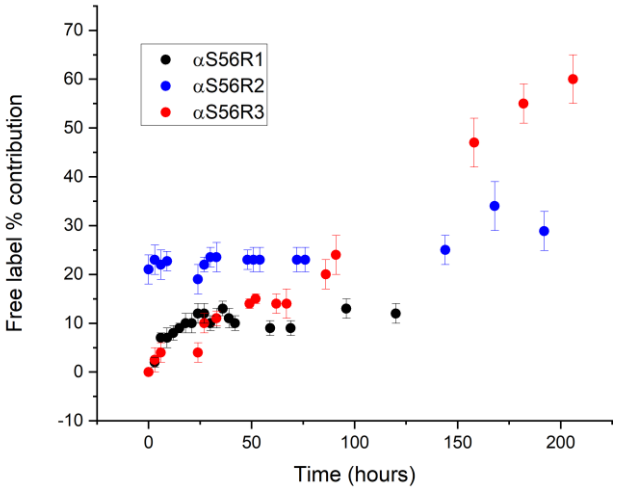

Figure 7. Free label contribution to the αS aggregation EPR spectra over time. Amount of free label in each spectrum is obtained by spectral simulation, see main text and materials and methods. Black: αS56R1. Red: αS56R2. Blue: αS56R3.

EPR spectral contributions can be used to obtain structural information. This requires that the aggregation-time course is not influenced by the label position. That is the case is proven by the ThT curves, where the aggregation process has the same time course, unaffected by the labels, proving that this condition is met (fig. 6C). Therefore, the observation that the slow component of αS9R1 reaches a plateau later than αS56R1 and αS27R1 suggests that position 9 does not take part in the initial fibrillization. Position 9 in fibrils is reported to be in the highly mobile tail end, outside of the fibril core, in agreement with this observation. On the other hand, position 27, which is closer to the fibril core but still outside of it, does not exhibit the same behavior as position 9. Perhaps its position close to the fibril core plays a role, however, the ultimate reason is unknown so far.

Next, we turn to the intermediates. As the fibril results suggest that time development of the EPR components can be used to obtain structural information, we apply it to the much more difficult to study intermediates of aggregation. In the time frame where oligomers occur, i.e. in the first 10-20 hours of the aggregation, αS27R1 is more immobilized than αS9R1 and αS56R1. This suggests that the region of αS around 27 is incorporated into the oligomers first, only to be followed by the regions around positions 9 and 56. Expanding this initial set of positions to other regions of αS could be expected to give a first indication about the location of residues in the oligomers, a first step to obtaining oligomer structure information.

Comparison of different labels

To probe spin labels with different linking groups, position 56 was labelled also with IAP (aS56R2) and MAP (aS56R3). Their respective linking groups have different chemical stabilities. While MTSL forms a disulfide bond that can be reduced, MAP and IAP form non-reducible bonds with the cysteine of the protein. Therefore, they can be used in the presence of reducing agents, like TCEP, required for some biomolecules to function in vitro. In MAP the bond is a thioether bond, in IAP a thioamide group (figure 2). Our results show that MTSL progressively detaches from the protein during the incubation, which is somewhat unexpected, because no reducing agent is added to the solution. While MAP behaves as expected, as it does not detach, it is unclear why IAP would detach in the time course of the aggregation. These results suggest to use MAP in situations where long incubations at relatively high temperature (37˚ C) are needed. Due to its higher stability, MAP is also a better choice for studies in reducing environments, like in cell studies, or partner interaction assays [29].

3.5 Conclusions

Overall, the data obtained so far highlight the strength of the in situ EPR approach in obtaining structural information on the intermediates of αS aggregation. This includes meta-stable, short lived species that would otherwise be removed from the solution with different approaches that involve chemical modification or dilution [14, 16-21]. By systematically applying in situ EPR with different label positions and comparing them, it could be possible to obtain site specific structural information on oligomeric species.

An additional possibility to gain more information is by allowing some exchange interaction to occur, if diamagnetic dilution is reduced. In this case exchange coupling becomes a major interaction in aggregates, and different degrees of diamagnetic dilution can be used to gain structural information as shown in [30, 31]. It is also possible that extending the method to higher EPR frequency, that provide better spectral resolution, would allow to observe τ_r differences between different label positions inside aggregates, and also to detect other mobility components that are hidden in the 9 GHz EPR nitroxide spectrum [32].

We demonstrate that the in situ EPR approach is a promising tool for studying αS aggregation, and for investigating transient intermediates that are otherwise difficult to capture. Future work could extend this method to higher EPR frequencies and additional label positions in αS, enhancing the capability to obtain site-specific structural insights into oligomeric species.

Supplementary Information

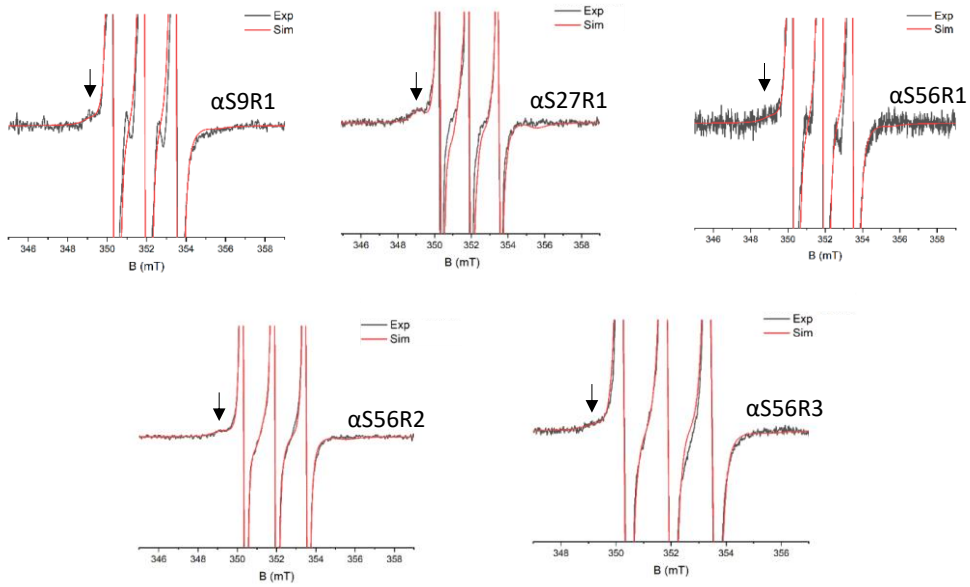

Figure SI.1. Zoom in on room temperature continuous wave EPR spectra of the different αS variants studied in this work. All spectra shown were acquired after six hours of aggregation. Black: experimental spectrum. Red: simulation. The arrows indicate the broad component, attributed to aggregates.

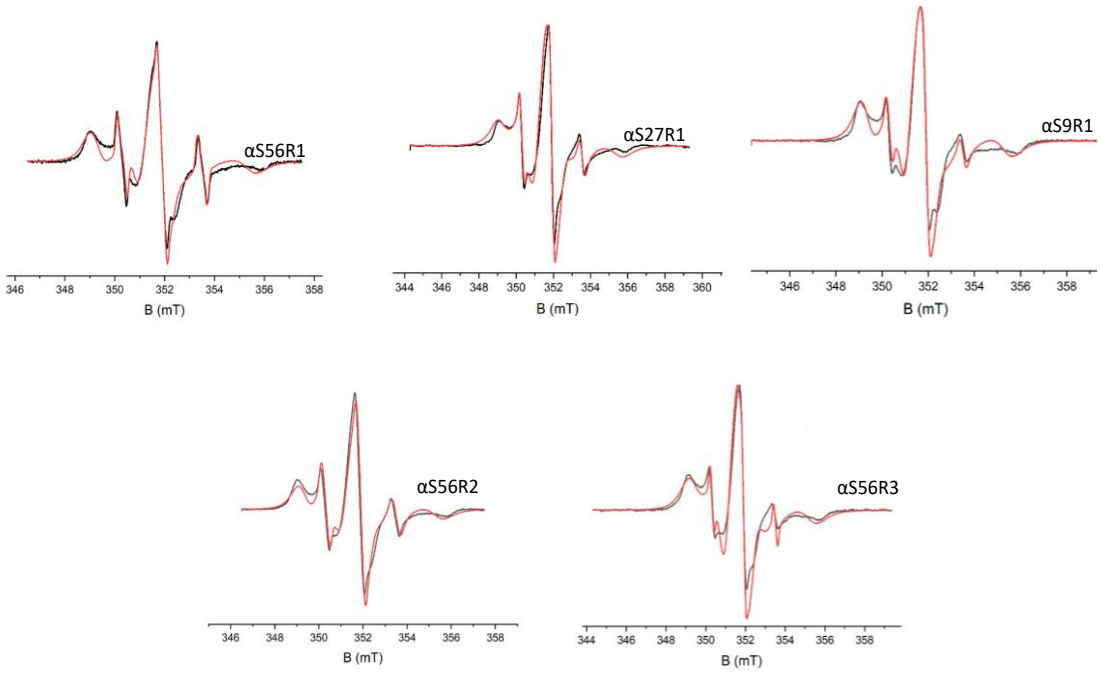

Figure SI.2. CW-EPR spectra obtained from fibril enriched samples. Black: experimental spectrum, red: simulation. For details, see main text.

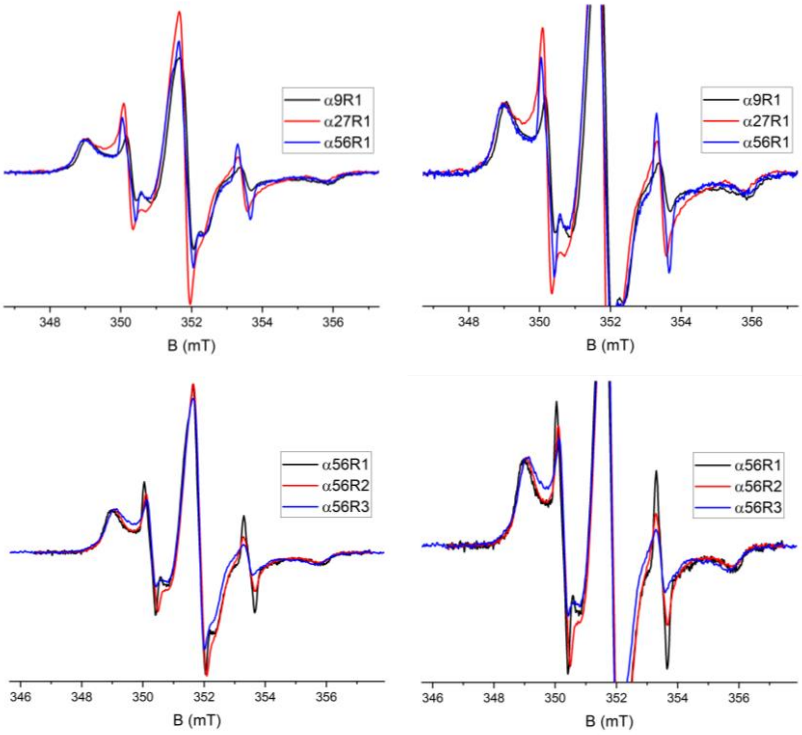

Figure SI.3. Comparison of experimental spectra obtained from fibril enriched samples from different mutants (upper two spectra) and different labels (lower two). The spectra are normalized to the intensity of the broad component around 349 mT. Left: full spectra, right: zoom in for better visualization.

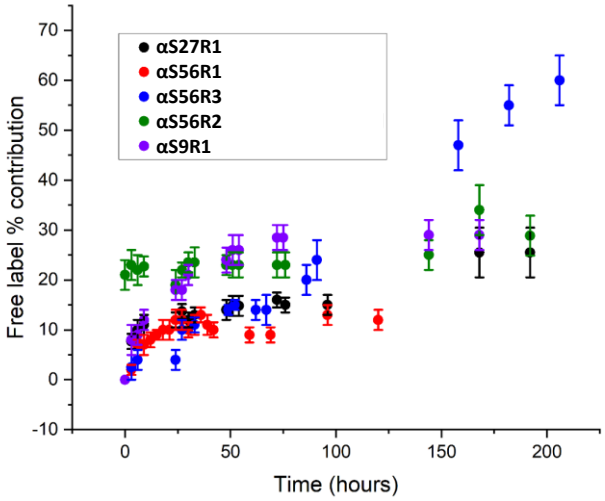

Figure SI.4 Free label contribution to the αS aggregation EPR spectra over time. Amount of free label in each spectrum is obtained by spectral simulation, see main text and materials and methods. Black: αS27R1. Red: αS56R1. Blue: αS56R3. Green: αS56R2. Purple: αS9R1

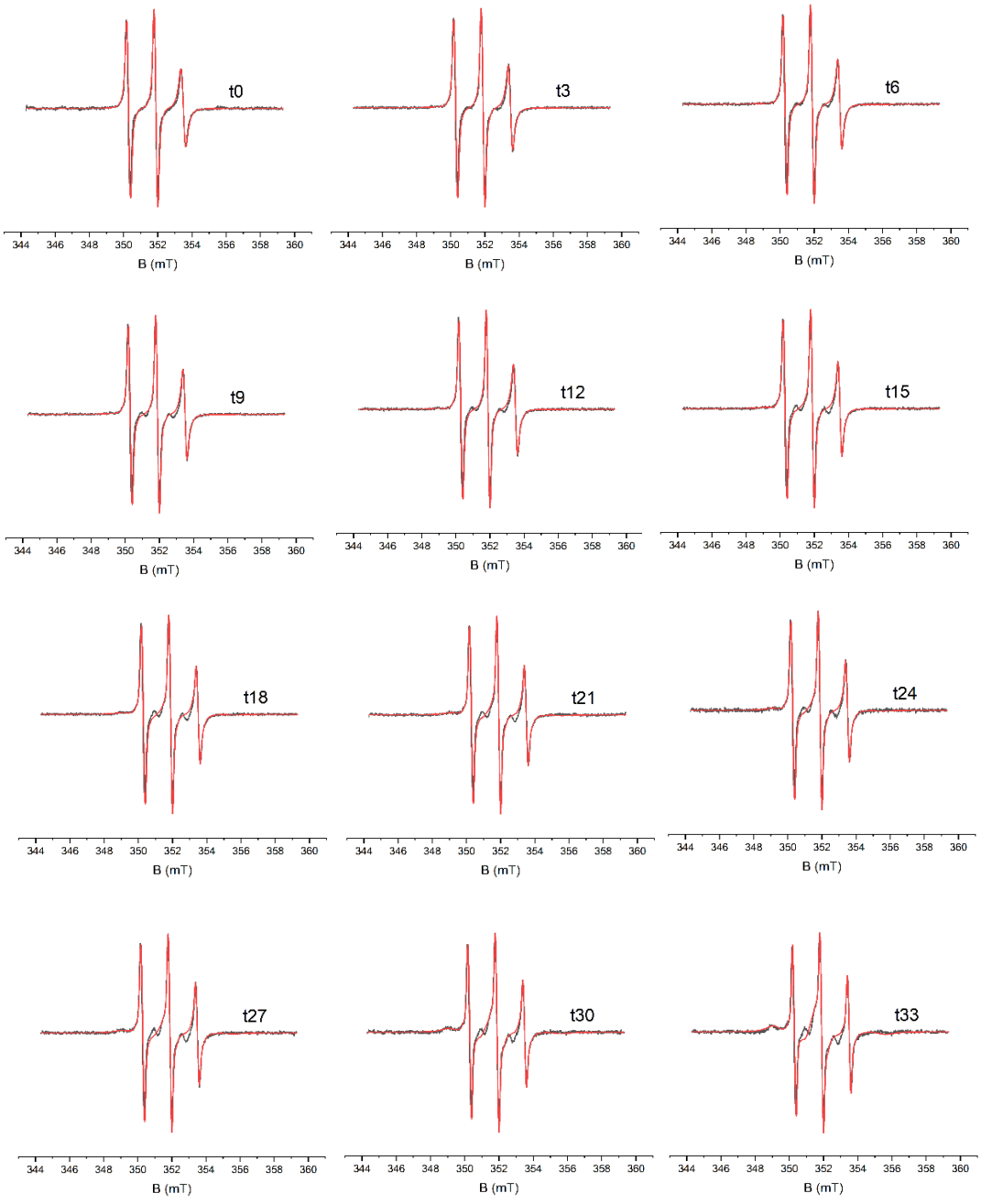
t0
t3
t6
t9
t12
t15
t18
t21
t24
t27
t30
t33
344 346 348 350 352 354 356 358 360
B (mT)

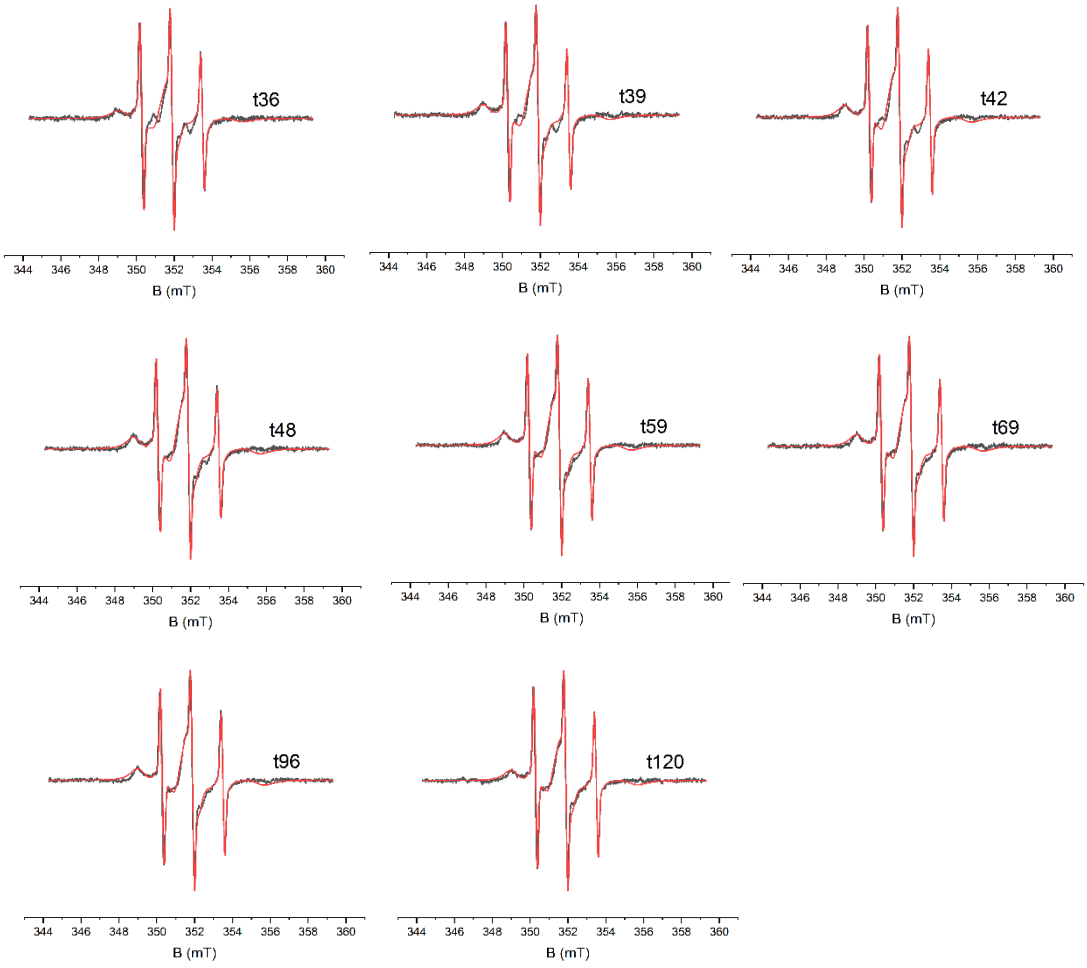

Figure SI.5. CW-EPR spectra obtained for αS56R1. Black: experimental spectrum. Red: simulation. The spectra presented for αS56R1 are the same as published in [25]. The simulations are updated to the method described in main text.

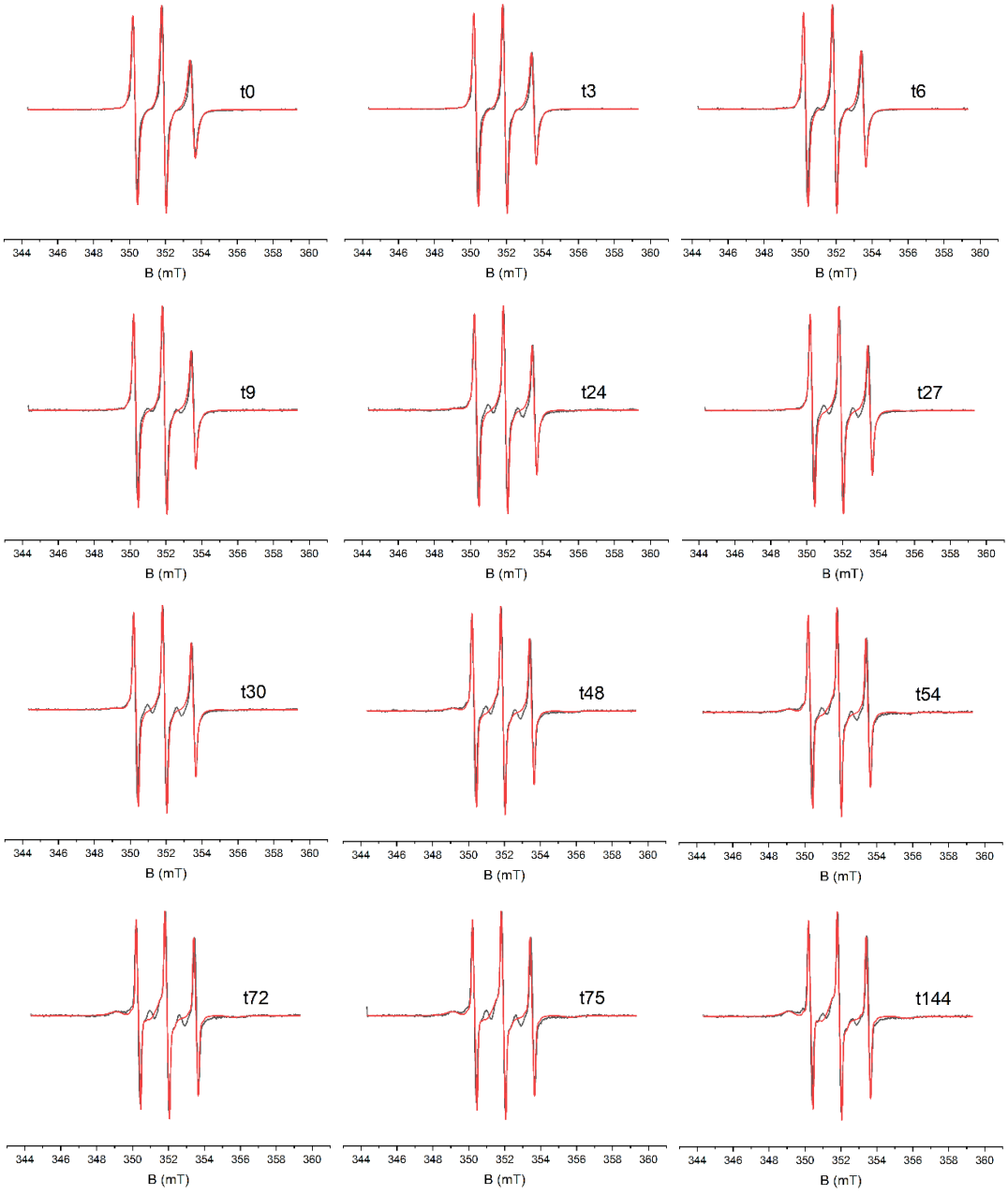
t0
t3
t6
t9
t24
t27
t30
t48
t54
t72
t75
t144
344 346 348 350 352 354 356 358 360
B (mT)

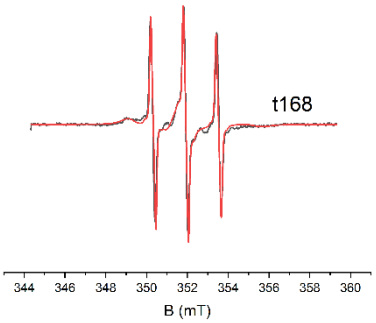

Figure SI.6. CW-EPR spectra obtained for αS9R1. Black: experimental spectrum. Red: simulation.

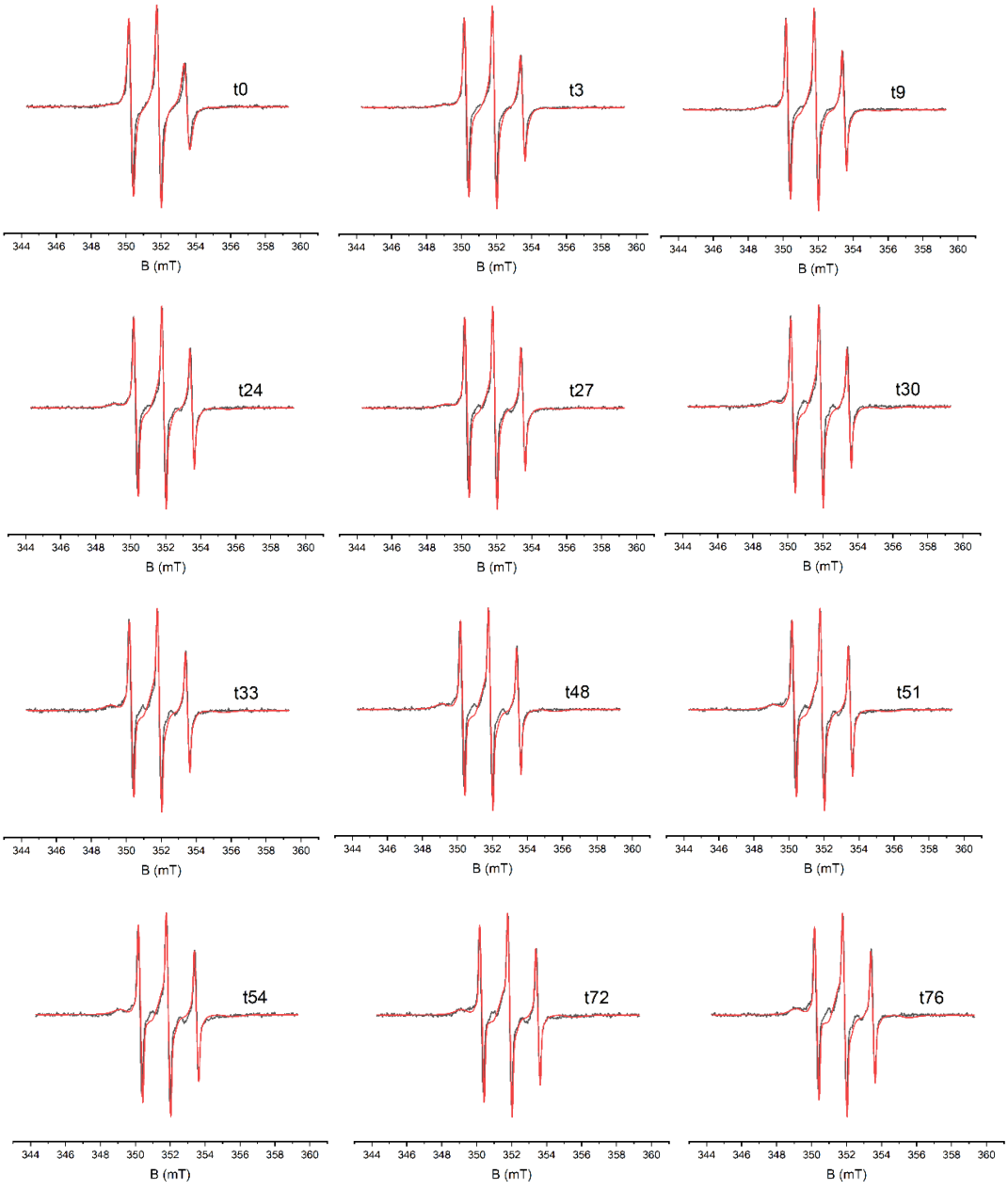
t0
t3
t9
t24
t27
t30
t33
t48
t51
t54
t72
t76
344 346 348 350 352 354 356 358 360
B (mT)

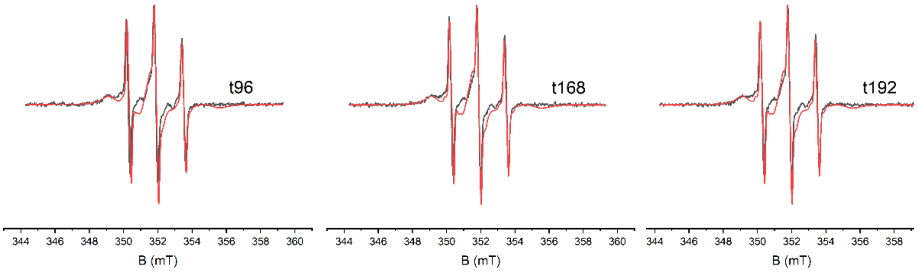

Fig. SI 7. CW-EPR spectra obtained for αS9R1. Black: experimental spectrum. Red: simulation.

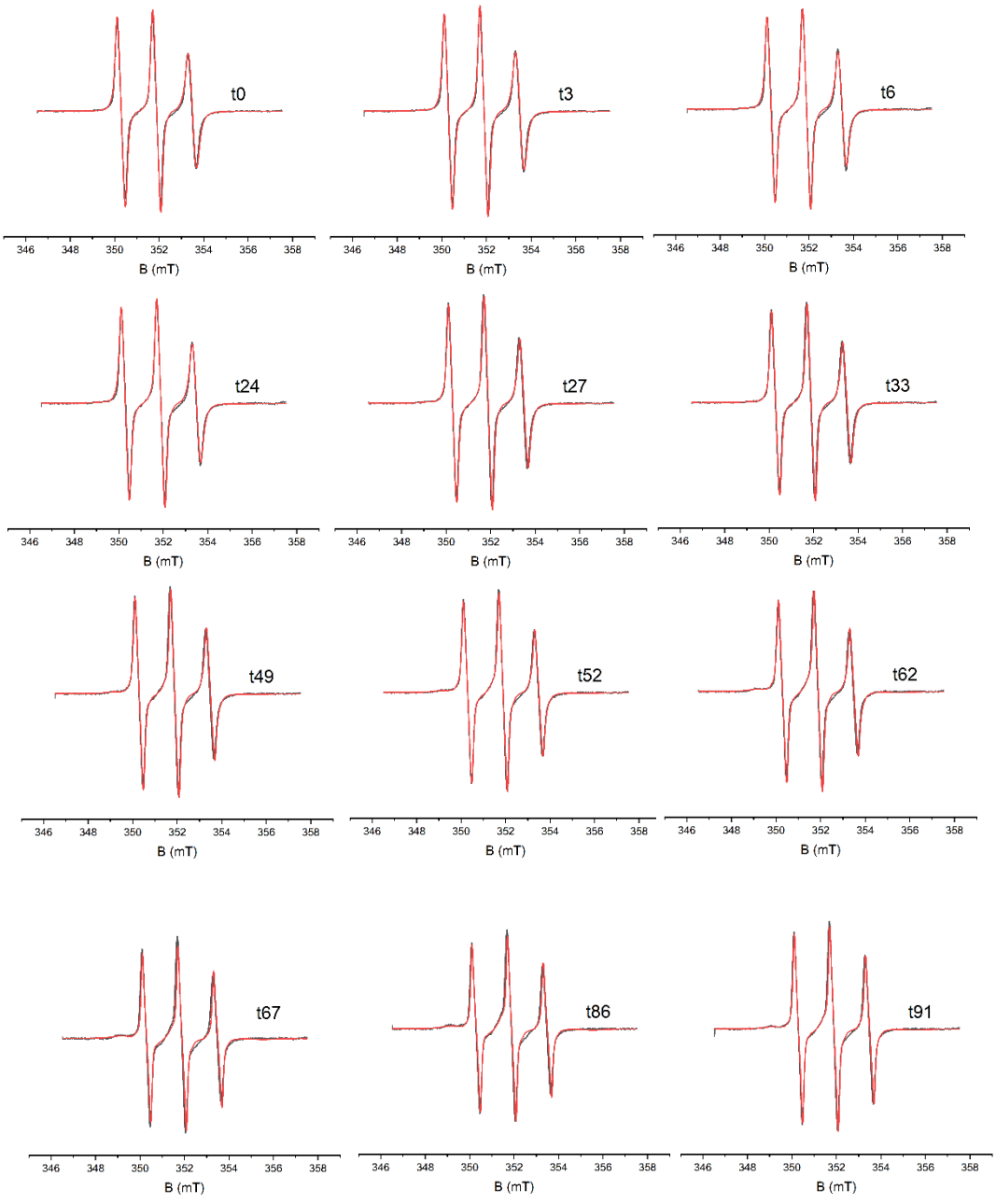
t0
t3
t6
t24
t27
t33
t49
t52
t62
t67
t86
t91
346 348 350 352 354 356 358
B (mT)

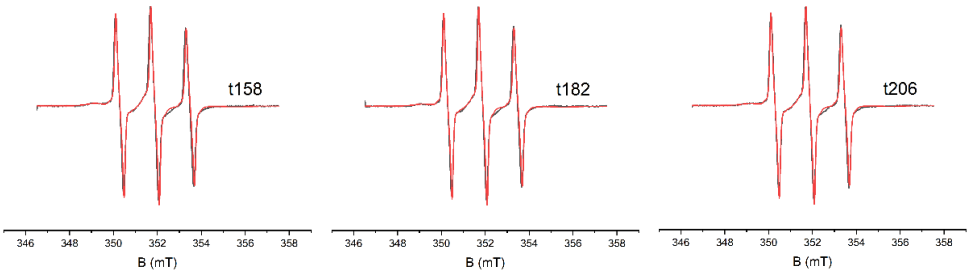

Figure SI.8. CW-EPR spectra obtained for αS56R2. Black: experimental spectrum. Red: simulation.

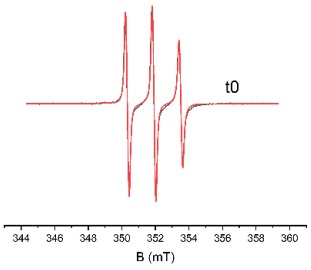
t0
344 346 348 350 352 354 356 358 360
B (mT)

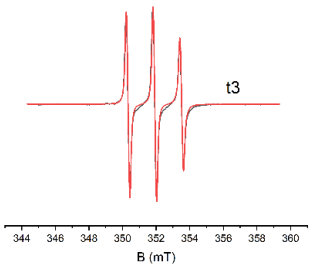
t3
344 346 348 350 352 354 356 358 360
B (mT)

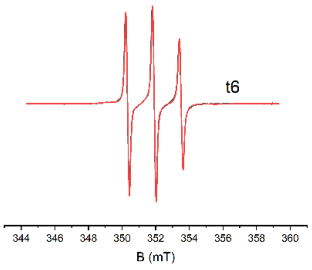
t6
344 346 348 350 352 354 356 358 360
B (mT)

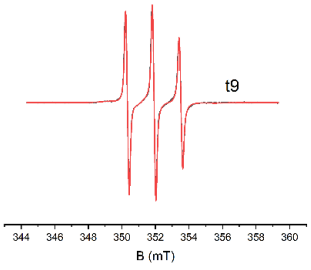
t9
344 346 348 350 352 354 356 358 360
B (mT)

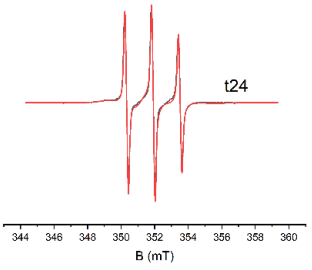
t24
344 346 348 350 352 354 356 358 360
B (mT)

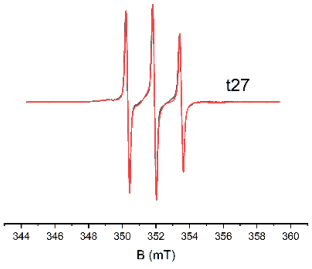
t27
344 346 348 350 352 354 356 358 360
B (mT)

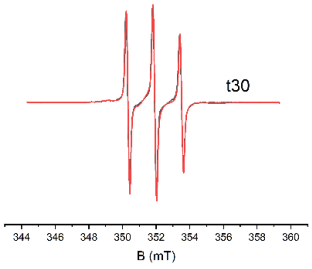
t30
344 346 348 350 352 354 356 358 360
B (mT)

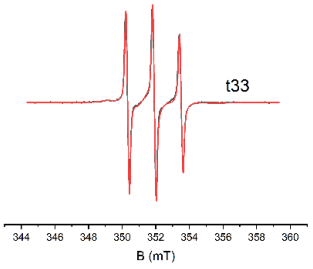
t33
344 346 348 350 352 354 356 358 360
B (mT)

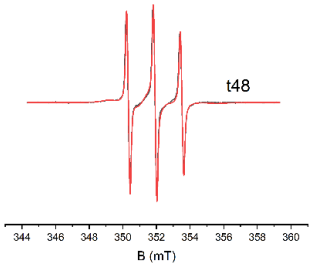
t48
344 346 348 350 352 354 356 358 360
B (mT)

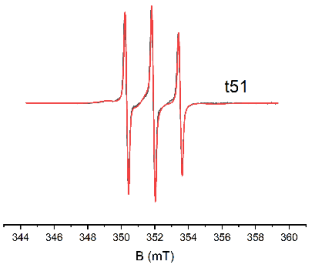
t51
344 346 348 350 352 354 356 358 360
B (mT)

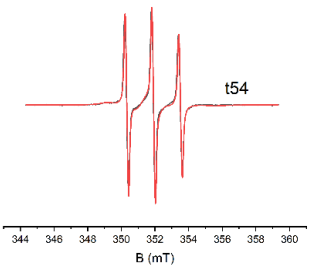
t54
344 346 348 350 352 354 356 358 360
B (mT)

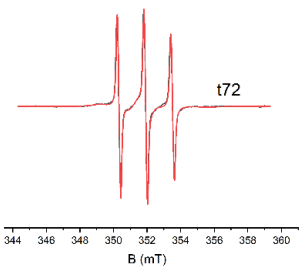
t72
344 346 348 350 352 354 356 358 360
B (mT)

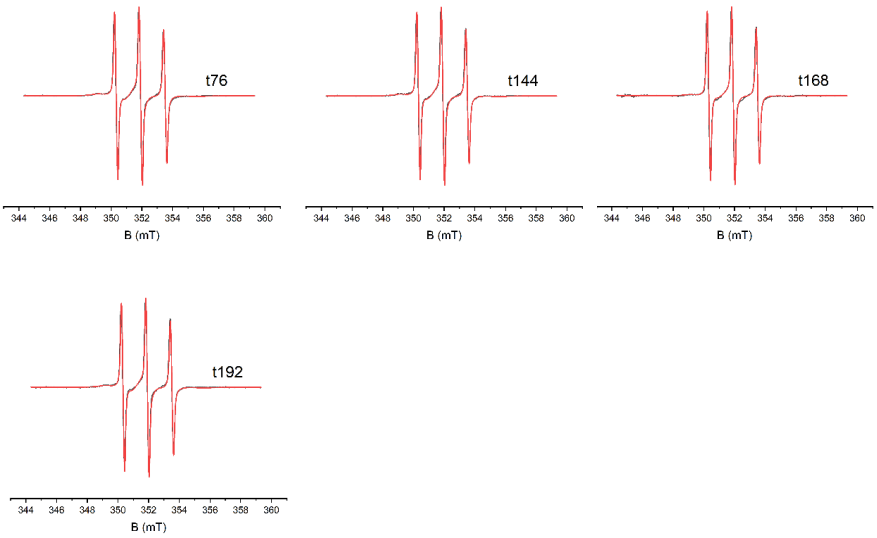

Figure SI.9. CW-EPR spectra obtained for αS56R3. Black: experimental spectrum. Red: simulation.

References

[1] L.M.A. Oliveira, T. Gasser, R. Edwards, M. Zweckstetter, R. Melki, L. Stefanis, H.A. Lashuel, D. Sulzer, K. Vekrellis, G.M. Halliday, J.J. Tomlinson, M. Schlossmacher, P.H. Jensen, J. Schulze-Hentrich, O. Riess, W.D. Hirst, O. El-Agnaf, B. Mollenhauer, P. Lansbury, T.F. Outeiro, Alpha-synuclein research: defining strategic moves in the battle against Parkinson's disease, npj Parkinson's Disease 7(1) (2021) 65.

[2] P. Calabresi, G. Di Lazzaro, G. Marino, F. Campanelli, V. Ghiglieri, Advances in understanding the function of alpha-synuclein: implications for Parkinson's disease, Brain 146(9) (2023) 3587-3597.

[3] A. Villar-Piqué, T. Lopes da Fonseca, T.F. Outeiro, Structure, function and toxicity of alpha-synuclein: the Bermuda triangle in synucleinopathies, Journal of Neurochemistry 139(S1) (2016) 240-255.

[4] P. Calabresi, A. Mechelli, G. Natale, L. Volpicelli-Daley, G. Di Lazzaro, V. Ghiglieri, Alpha-synuclein in Parkinson's disease and other synucleinopathies: from overt neurodegeneration back to early synaptic dysfunction, Cell Death & Disease 14(3) (2023) 176.

[5] P. Arosio, T.P.J. Knowles, S. Linse, On the lag phase in amyloid fibril formation, Physical Chemistry Chemical Physics 17(12) (2015) 7606-7618.

[6] N. Bengoa-Vergniory, R.F. Roberts, R. Wade-Martins, J. Alegre-Abarrategui, Alpha-synuclein oligomers: a new hope, Acta Neuropathologica 134(6) (2017) 819-838.

[7] M.D. Tuttle, G. Comellas, A.J. Nieuwkoop, D.J. Covell, D.A. Berthold, K.D. Kloepper, J.M. Courtney, J.K. Kim, A.M. Barclay, A. Kendall, W. Wan, G. Stubbs, C.D. Schwieters, V.M.Y. Lee, J.M. George, C.M. Rienstra, Solid-state NMR structure of a pathogenic fibril of full-length human α-synuclein, Nature Structural & Molecular Biology 23(5) (2016) 409-415.

[8] J. Gath, L. Bousset, B. Habenstein, R. Melki, B.H. Meier, A. Bockmann, Yet another polymorph of alpha-synuclein: solid-state sequential assignments, Biomol NMR Assign 8(2) (2014) 395-404.

[9] J. Gath, B. Habenstein, L. Bousset, R. Melki, B.H. Meier, A. Böckmann, Solid-state NMR sequential assignments of α-synuclein, Biomolecular NMR Assignments 6(1) (2012) 51-55.

[10] J. Verasdonck, L. Bousset, J. Gath, R. Melki, A. Bockmann, B.H. Meier, Further exploration of the conformational space of alpha-synuclein fibrils: solid-state NMR assignment of a high-pH polymorph, Biomol NMR Assign 10(1) (2016) 5-12.

[11] R. Guerrero-Ferreira, N.M. Taylor, A.A. Arteni, P. Kumari, D. Mona, P. Ringler, M. Britschgi, M.E. Lauer, A. Makky, J. Verasdonck, R. Riek, R. Melki, B.H. Meier, A. Bockmann, L. Bousset, H. Stahlberg, Two new polymorphic structures of human full-length alpha-synuclein fibrils solved by cryo-electron microscopy, Elife 8 (2019).

[12] R. Guerrero-Ferreira, L. Kovacik, D. Ni, H. Stahlberg, New insights on the structure of alpha-synuclein fibrils using cryo-electron microscopy, Curr Opin Neurobiol 61 (2020) 89-95.

[13] R. Guerrero-Ferreira, N.M. Taylor, D. Mona, P. Ringler, M.E. Lauer, R. Riek, M. Britschgi, H. Stahlberg, Cryo-EM structure of alpha-synuclein fibrils, Elife 7 (2018).
[14] N. Lorenzen, S.B. Nielsen, A.K. Buell, J.D. Kaspersen, P. Arosio, B.S. Vad, W. Paslawski, G. Christiansen, Z. Valnickova-Hansen, M. Andreasen, J.J. Enghild, J.S. Pedersen, C.M. Dobson, T.P. Knowles, D.E. Otzen, The role of stable alpha-synuclein oligomers in the molecular events underlying amyloid formation, J Am Chem Soc 136(10) (2014) 3859-68.
[15] P. Alam, L. Bousset, R. Melki, D.E. Otzen, α-synuclein oligomers and fibrils: a spectrum of species, a spectrum of toxicities, Journal of Neurochemistry 150(5) (2019) 522-534.
[16] N. Cremades, Samuel I.A. Cohen, E. Deas, Andrey Y. Abramov, Allen Y. Chen, A. Orte, M. Sandal, Richard W. Clarke, P. Dunne, Francesco A. Aprile, Carlos W. Bertoncini, Nicholas W. Wood, Tuomas P.J. Knowles, Christopher M. Dobson, D. Klenerman, Direct Observation of the Interconversion of Normal and Toxic Forms of α-Synuclein, Cell 149(5) (2012) 1048-1059.
[17] S.W. Chen, S. Drakulic, E. Deas, M. Ouberai, F.A. Aprile, R. Arranz, S. Ness, C. Roodveldt, T. Guilliams, E.J. De-Genst, D. Klenerman, N.W. Wood, T.P. Knowles, C. Alfonso, G. Rivas, A.Y. Abramov, J.M. Valpuesta, C.M. Dobson, N. Cremades, Structural characterization of toxic oligomers that are kinetically trapped during alpha-synuclein fibril formation, Proc Natl Acad Sci U S A 112(16) (2015) E1994-2003.
[18] I. Pérez-Pi, D.A. Evans, M.H. Horrocks, N.T. Pham, K.S. Dolt, J. Koszela, T. Kunath, M. Auer, α-Synuclein–Confocal Nanoscanning (ASYN-CONA), a Bead-Based Assay for Detecting Early-Stage α-Synuclein Aggregation, Analytical Chemistry 91(9) (2019) 5582-5590.
[19] L. Zhou, D. Kurouski, Structural Characterization of Individual α-Synuclein Oligomers Formed at Different Stages of Protein Aggregation by Atomic Force Microscopy-Infrared Spectroscopy, Analytical Chemistry 92(10) (2020) 6806-6810.
[20] F. van Diggelen, D. Hrle, M. Apetri, G. Christiansen, G. Rammes, A. Tepper, D.E. Otzen, Two conformationally distinct alpha-synuclein oligomers share common epitopes and the ability to impair long-term potentiation, PLoS One 14(3) (2019) e0213663.
[21] J.I. Gallea, M.S. Celej, Structural Insights into Amyloid Oligomers of the Parkinson Disease-related Protein α-Synuclein*, Journal of Biological Chemistry 289(39) (2014) 26733-26742.
[22] K. Gade Malmos, L.M. Blancas-Mejia, B. Weber, J. Buchner, M. Ramirez-Alvarado, H. Naiki, D. Otzen, ThT 101: a primer on the use of thioflavin T to investigate amyloid formation, Amyloid 24(1) (2017) 1-16.
[23] H. Naiki, K. Higuchi, M. Hosokawa, T. Takeda, Fluorometric determination of amyloid fibrils in vitro using the fluorescent dye, thioflavine T, Analytical Biochemistry 177(2) (1989) 244-249.
[24] H. LeVine, [18] Quantification of β-sheet amyloid fibril structures with thioflavin T, Methods in Enzymology, Academic Press1999, pp. 274-284.

[25] E. Zurlo, P. Kumar, G. Meisl, A.J. Dear, D. Mondal, M.M.A.E. Claessens, T.P.J. Knowles, M. Huber, In situ kinetic measurements of α-synuclein aggregation reveal large population of short-lived oligomers, PLOS ONE 16(1) (2021) e0245548.
[26] E. Zurlo, L. Passerini, P. Kumar, M. Huber, In Situ Continuous Wave Electron Paramagnetic Resonance Investigation of the Amyloid Aggregation of Parkinson's Protein Alpha-Synuclein—the Second Spin-Label Position, Applied Magnetic Resonance 53(7) (2022) 1133-1150.
[27] T. Ikenoue, Y.-H. Lee, J. Kardos, M. Saiki, H. Yagi, Y. Kawata, Y. Goto, Cold Denaturation of α-Synuclein Amyloid Fibrils, Angewandte Chemie International Edition 53(30) (2014) 7799-7804.
[28] S. Stoll, A. Schweiger, EasySpin, a comprehensive software package for spectral simulation and analysis in EPR, J Magn Reson 178(1) (2006) 42-55.
[29] A. Bonucci, O. Ouari, B. Guigliarelli, V. Belle, E. Mileo, In-Cell EPR: Progress towards Structural Studies Inside Cells, Chembiochem 21(4) (2020) 451-460.
[30] H. Xiao, L. Duo, J. Zhen, H. Wang, Z. Guo, Static and dynamic disorder in Aβ40 fibrils, Biochemical and Biophysical Research Communications 610 (2022) 107-112.
[31] M. Chen, M. Margittai, J. Chen, R. Langen, Investigation of alpha-synuclein fibril structure by site-directed spin labeling, J Biol Chem 282(34) (2007) 24970-9.
[32] E. Zurlo, I. Gorroño Bikandi, N.J. Meeuwenoord, D.V. Filippov, M. Huber, Tracking amyloid oligomerization with monomer resolution using a 13-amino acid peptide with a backbone-fixed spin label, Physical Chemistry Chemical Physics 21(45) (2019) 25187-25195.